

# Surface wave tomography of North America and the Caribbean using global and regional broad-band networks: phase velocity maps and limitations of ray theory

Stéphanie Godey,<sup>1</sup> Roel Snieder,<sup>1,\*</sup> Antonio Villaseñor<sup>1,2</sup> and Harley M. Benz<sup>2</sup>

<sup>1</sup>Faculty of Earth Sciences, Utrecht University, PO Box 80021, 3508 TA Utrecht, The Netherlands. E-mail: godey@geo.uu.nl

<sup>2</sup>US Geological Survey, Box 25046, MS 966, Denver Federal Center, Denver, CO 80225, USA

Accepted 2002 September 6. Received 2002 July 31; in original form 2002 January 8

## SUMMARY

We present phase velocity maps of fundamental mode Rayleigh waves across the North American and Caribbean plates. Our data set consists of 1846 waveforms from 172 events recorded at 91 broad-band stations operating in North America. We compute phase velocity maps in four narrow period bands between 50 and 150 s using a non-linear waveform inversion method that solves for phase velocity perturbations relative to a reference Earth model (PREM). Our results show a strong velocity contrast between high velocities beneath the stable North American craton, and lower velocities in the tectonically active western margin, in agreement with other regional and global surface wave tomography studies. We perform detailed comparisons with global model results, which display good agreement between phase velocity maps in the location and amplitude of the anomalies. However, forward modelling shows that regional maps are more accurate for predicting waveforms. In addition, at long periods, the amplitude of the velocity anomalies imaged in our regional phase velocity maps is three times larger than in global phase velocity models. This amplitude factor is necessary to explain the data accurately, showing that regional models provide a better image of velocity structures. Synthetic tests show that the raypath coverage used in this study enables one to resolve velocity features of the order of 800–1000 km. However, only larger length-scale features are observed in the phase velocity maps. The limitation in resolution of our maps can be attributed to the wave propagation theory used in the inversion. Ray theory does not account for off-great-circle ray propagation effects, such as ray bending or scattering. For wavelengths less than 1000 km, scattering effects are significant and may need to be considered.

**Key words:** Caribbean, North America, phase velocity, ray theory, scattering, surface wave tomography.

## 1 INTRODUCTION

The main goal of this study is to obtain better phase velocity maps with improved lateral resolution across North America using the extensive surface wave database available nowadays. In the previous decades, the number of high-quality broad-band seismic stations deployed in the region has increased considerably. In addition to the global and national networks, the North American continent and, in particular, the United States will be densely covered in the near future with permanent and temporary seismic stations from the ANSS (USGS 1999) and USArray (Levander *et al.* 1999) projects. Consequently, high-resolution velocity models of the region are expected to be derived from this extensive data collection. The present re-

search investigates how the increasing density of seismic stations improves the imaging of the velocity structure.

This study, covering the entire North American Plate, attempts to close the gap between local and global tomography studies. The latest surface wave investigations of North America were performed for subregions of the continent: Canada (Frederiksen *et al.* 2001), the Arctic region (Levshin *et al.* 2001), and the continental United States (Alsina *et al.* 1996; Van der Lee & Nolet 1997). Alsina *et al.* (1996) imaged the United States with a smaller data set, using the same method applied here, followed by a linear inversion that included scattering effects. Van der Lee & Nolet (1997) and Frederiksen *et al.* (2001) used the partitioned waveform inversion method of Nolet (1990). As this method includes higher-mode Rayleigh waves, deeper velocity structures are imaged.

The sensitivity of the fundamental mode Rayleigh waves for the periods considered in this study allows one to relate phase velocity

\*Now at: Department of Geophysics, Colorado School of Mines, Golden, CO, 80401-1887, USA.

maps to shear velocity structure, which can be correlated to features in the uppermost mantle (e.g. Curtis *et al.* 1998).

Another application of phase velocity maps is the determination of source mechanisms using moment tensor inversion methods (e.g. the centroid moment tensor (CMT) method). Even for globally recorded large earthquakes, corrections for the aspherical Earth structure need to be taken into account (Dziewonski *et al.* 1992), although long-wavelength 3-D velocity models are generally sufficient (e.g. Woodhouse & Dziewonski 1984). However, for smaller events, higher-resolution models are required to predict surface wave traveltimes with the necessary accuracy (Arvidsson & Ekström 1998; Pasyanos *et al.* 1996). This study should provide phase velocity maps of North America with the appropriate resolution for this application.

In this study, we also perform a detailed comparison of regional and global models in terms of velocity structures and resolution. Chevrot *et al.* (1998) and Larson & Ekström (2001) previously analysed the agreements between global and regional models. A systematic underestimation of velocity amplitude is observed in global models (Nolet *et al.* 1994; Larson & Ekström 2001). Here we compare, in particular, our velocity maps with the global model of Trampert & Woodhouse (2001).

## 2 DATA

The waveforms used in this study were extracted from seismograms recorded between 1995 and 1999 by a number of global and regional

networks: Global Seismograph Network (GSN), Geoscope, US National Seismograph Network (USNSN), Canadian National Seismic Network (CNSN), Berkeley Digital Seismic Network (BDSN), TERRAscope and other individual stations in North America. In total, we collected waveforms for 172 events recorded by a subset of 91 permanent broad-band stations. In California, where a large number of broad-band stations are available, only a subset of well-distributed stations was selected. The earthquake source parameters were taken from the Harvard Centroid Moment Tensor catalogue (Dziewonski & Anderson 1981). The earthquakes used were all shallow, most of them being located at crustal depths. We first measured group velocities for the fundamental mode Rayleigh waves using an implementation of the time–frequency analysis method (e.g. Levshin *et al.* 1992) developed by Charles Ammon, which is described in Pasyanos *et al.* (2001). In order to select only the fundamental mode Rayleigh wave and eliminate heavily scattered energy (coda) and higher modes, we apply a phase-matched filter that uses the group velocity information. The resulting clean seismograms are used in the non-linear waveform inversion. We only selected seismograms for which we were able to obtain reliable group velocity measurements in the complete period range 50–150 s. As a result, the source–receiver geometry is identical for all periods and consists of 1846 raypaths. Fig. 1 shows the distribution of seismic sources, stations and raypath coverage used in this study. Well-distributed seismic sources and stations throughout the region result in homogeneous raypath coverage over most of North America, except for the Arctic Ocean and the easternmost part of the Caribbean basin and

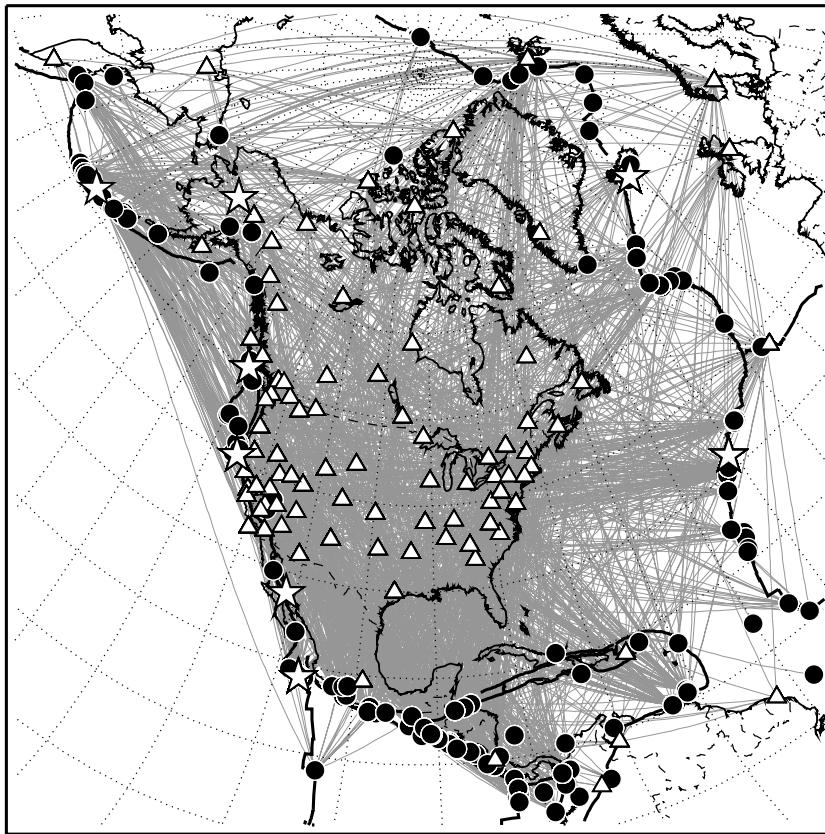


**Figure 1.** Study area showing the distribution of broad-band seismic stations (open triangles) and earthquakes (solid circles) used to determine variations in phase velocity across North America. The great circle paths sampling the area are depicted by grey lines. Also labelled are the events recorded in 2000 (stars) and used in the forward modelling of Section 6.1.

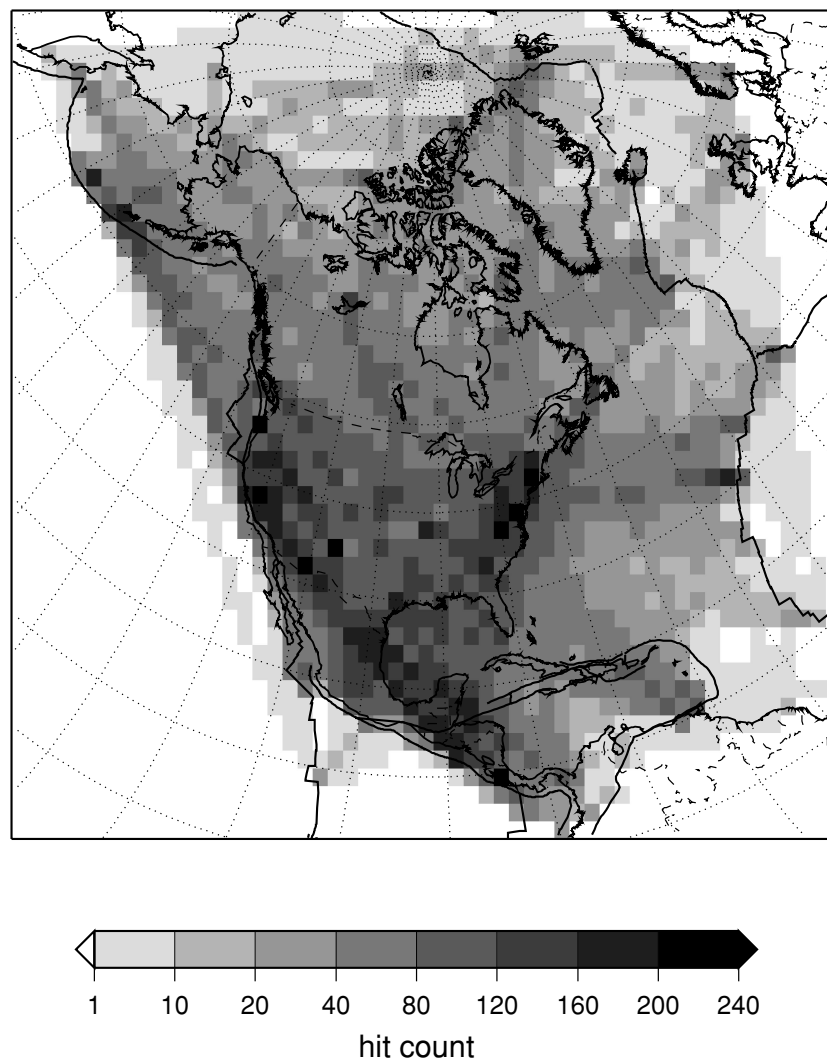


**Figure 2.** Map of ray density within the study region. The ray density is defined as the number of rays crossing each  $2 \times 2 \text{ deg}^2$  cell.

Mid-Atlantic ridge. This coverage represents a large improvement with respect to previous surface wave studies of North America: 275 recordings used in Alsina *et al.* (1996) and 685 in Van der Lee & Nolet (1997).

While raypath coverage provides insight into the areas that can be imaged, raypath density provides more details on how well the region is sampled. The raypath density map shown in Fig. 2 is calculated as the number of rays hitting each  $2 \times 2 \text{ deg}^2$  cell. The entire continental United States and the Gulf of Mexico are well sampled, while poorer sampling is observed around the edges of the studied region.

### 3 INVERSION METHOD

The procedure used in this work is based on a non-linear iterative inversion method developed by Nolet *et al.* (1986) for waveform fitting. The same inversion technique was previously applied by Alsina *et al.* (1996) to the United States. The phase velocity maps are computed by minimizing a penalty function in the time domain (Snieder 1988) through eq. (1):

$$F(m) = \sum_{i=1}^N \int [u_i(t) - s_i(m, t)]^2 dt + \gamma \int |\nabla_h m|^2 dW. \quad (1)$$

The  $N$  synthetic seismograms  $s_i$  are computed through the predicted phase velocity model  $m$  and are compared with the observed seismograms  $u_i$ . The minimization is achieved using a conjugate gradient method. A smoothing constraint related to the horizontal gradient of the model  $|\nabla_h|^2$  is applied. The damping parameter  $\gamma$  is chosen to find the optimal trade-off between model smoothness and data fit. The study region covers an area of  $10\,340 \times 12\,100 \text{ km}^2$ , which consists of  $48 \times 56$  nodes distributed over a rectangular grid of  $2^\circ$  spacing. At each gridpoint of the model  $m$ , phase velocity perturbations  $\delta c/c$  relative to the reference model PREM (Dziewonski & Anderson 1981) are computed. The phase velocities between the nodes are interpolated using bicubic splines. Synthetic seismograms that fit the data poorly after a preliminary inversion are removed, resulting in the elimination of 17 per cent of the original data set. The distribution of the discarded paths does not present any systematic relation to a specific source or station.

We carry out the inversion in three steps in order to obtain smooth convergence towards the minimum of the penalty function. First, we solve for velocity perturbations by inverting the normalized envelope of the waveforms, which is insensitive to cycle skipping. This step is equivalent to inverting for group velocities and provides a model that fits the overall phase observations without considering

the contribution of both amplitude and phase. Secondly, the normalized waveforms of the seismograms, which contain phase information, are inverted. Finally, the true waveforms (i.e. not normalized for amplitude) containing amplitude and phase information are inverted to obtain the final phase velocity maps. For each of the three steps, ten iterations are performed. The value of the damping parameter ( $\gamma = 0.01$ ) is identical for all periods and for each of the three inversion steps. The waveforms are extracted and inverted individually over four narrow period bands: 50–66, 66–88, 88–115 and 115–150 s. The width of the period bands is calculated in order to obtain equal spacing in both period and frequency logarithms ( $\ln dT = 0.26$ ). In each period band, we assume a constant relative phase velocity perturbation. For the 115–150 s period band, PREM was used as a starting model. The phase velocity map obtained for the 115–150 s period band was used as the starting model of the inversion in the 88–115 s period band. This process is applied to successively shorter period bands.

#### 4 RESOLUTION TESTS AND ERROR ESTIMATES

The raypath coverage and ray density per cell (Figs 1 and 2) provide a qualitative insight into the resolution of the model. For a more quantitative analysis, we perform chequerboard and spike anomaly tests. First, an input model is created and synthetic seismograms are computed by forward modelling through the given model using the source and receiver geometry of this study (Fig. 1). The resulting synthetic data set is then inverted using the same procedure and model parametrization described above. Comparing the input model with its reconstruction provides an assessment of model resolution, in particular on the amplitude, location and size of the velocity anomalies. Lévêque *et al.* (1993) showed that these tests could be misleading for certain parametrizations and source–receiver configurations. In our case, the well-distributed combination of sources and stations should not lead to this problem. We perform several tests for input anomalies of different size and location. The ideal case would be to perform a spike test on each cell of the model, providing information on point-by-point resolution as performed by Ritzwoller & Levshin (1998). However, this is not practical given the size of our model, which consists of 2688 grid points.

To illustrate the synthetic experiments, chequerboard and spike test results corresponding to the 66–88 s period band are displayed in Figs 3 and 4. Similar results are observed for all periods with minor degradation at longer periods. The left-hand panels of Figs 3 and 4 show the input velocity models used and the right-hand panels present the reconstructed models after inversion. Alternating velocity perturbations of +5 and –5 per cent are used to produce a chequerboard pattern on which we applied a sinusoidal smoothing. Chequerboard tests for velocity anomalies of 16°, 12° and 8° are shown in Figs 3(a), (b) and (c), (d) and 4(a), (b), respectively. The chequerboard shown in Figs 3(c) and (d) is rotated by 45° compared with the others (Figs 3a, b and 4a, b) in order to assess the influence of azimuthal coverage. The 8° spike test is displayed in Figs 4(c) and (d) and consists of five discrete anomalies characterized by an amplitude variation of +5 per cent. The distribution of the anomalies is similar to that used by Van der Lee & Nolet (1997) with an additional anomaly located beneath Iceland.

The spatial location and the amplitude of the anomalies are well recovered in our synthetic reconstructions in most of the study area. All reconstructed models display lower resolution along the edges of the target area, where anomalies are smeared out because of limited ray coverage and poor azimuthal sampling. Alsina *et al.*

(1996) observed in their phase velocity maps a bias toward smaller reconstructed amplitudes, which they attributed to the smoothing parameter used in the inversion. In our study, the data set is six times larger, required lower smoothing and, as a result we achieve a better reconstruction of the amplitude of the synthetic anomalies.

For the long-wavelength anomalies, a good match in amplitude and location is achieved across the entire North American continent and the Caribbean. In Greenland, Iceland and in the Pacific and Atlantic oceans reconstruction is poorer owing to the lack of crossing rays. For intermediate and small wavelengths (12° and 8°, Figs 3c, d and 4a,b), reconstruction discrepancies between regions are observed. Beneath the continental United States, the amplitude and location of the chequerboard patterns are still well recovered. For the rest of the study area, the resolving power for 12° and 8° anomalies is lower and is related to inadequate ray sampling. In the Caribbean, smearing occurs in an E–W direction (Fig. 3d), and for Canada, Alaska and the Arctic we obtain low resolution. For the 8° anomalies, we reconstruct the locations of the heterogeneities well, but the amplitudes are 30 per cent lower on average. Figs 4(c) and (d) show results for the five discrete spike anomalies. In the continent, all four anomalies are well reconstructed in amplitude (100 per cent at the centre of the spike) and location. For the same test, the model obtained by Van der Lee & Nolet (1997) displays underestimated amplitudes (a maximum of 60 per cent at the centre of the spike). However, the anomaly beneath Iceland is slightly shifted to the southwest by approximately 1000 km owing to poor sampling in the region. These results show that the source–receiver geometry is adequate for imaging structures of down to approximately 800 km in the continental United States and in most of the North American continent.

Another measure of the performance of our inversion is the variance reduction, which is computed for each period band using

$$\text{variance reduction (per cent)} = \left[ 1 - \frac{\sum_{i=1}^N (u_i - s_i)^2}{\sum_{i=1}^N (u_i - u_i^0)^2} \right] \times 100, \quad (2)$$

where  $N$  is the number of seismograms,  $u_i^0$  is the synthetic seismogram computed through the laterally homogeneous model (PREM),  $u_i$  is the observed waveform (data) and  $s_i$  is the synthetic seismogram computed using the model obtained from the inversion. The variance reduction for each of the period bands is shown in Table 1. The variance reduction decreases systematically for shorter periods as a result of the complexity of the waveforms. Overall, from 50 to 150 s, the non-linear inversion accounts for up to a 70 per cent reduction in variance. This represents a substantial improvement with respect to the study of Alsina *et al.* (1996) for which the maximum variance reduction was 40 per cent. As mentioned previously, final synthetics presenting a worse fit than the initial synthetics (PREM) are excluded from the final inversion. In this process, 380 seismograms were eliminated. In Fig. 5, we show an example of waveform fits for one event at all period bands. The initial synthetic seismograms computed through the homogeneous starting model (PREM) predict poorly both the amplitude and phase of the observed data. After the three-step inversion, both the amplitude and the phase of the observed seismogram are well matched by the synthetic seismogram.

#### 5 INVERSION RESULTS

Fig. 6 shows the phase velocity maps obtained for the four period bands considered: 115–150, 88–115, 66–88 and 50–66 s. Our results

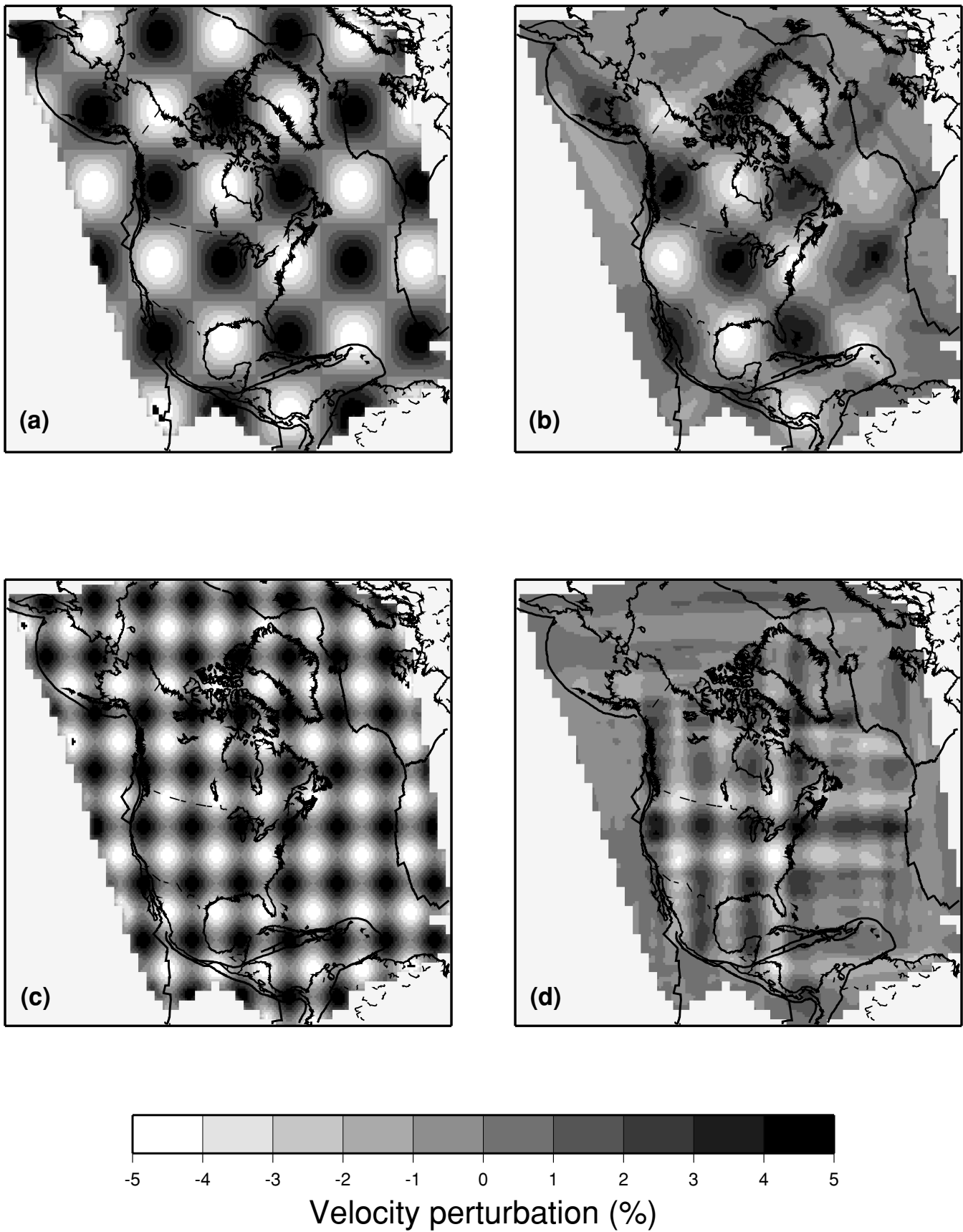


**Figure 3.** Results of the resolution tests: input (a, c) and output (b, d) phase velocity maps of the sensitivity tests for the period band 66–88 s. Cell sizes of the checkerboards are 16° (a, b) and 12° with transversal orientation (c, d).

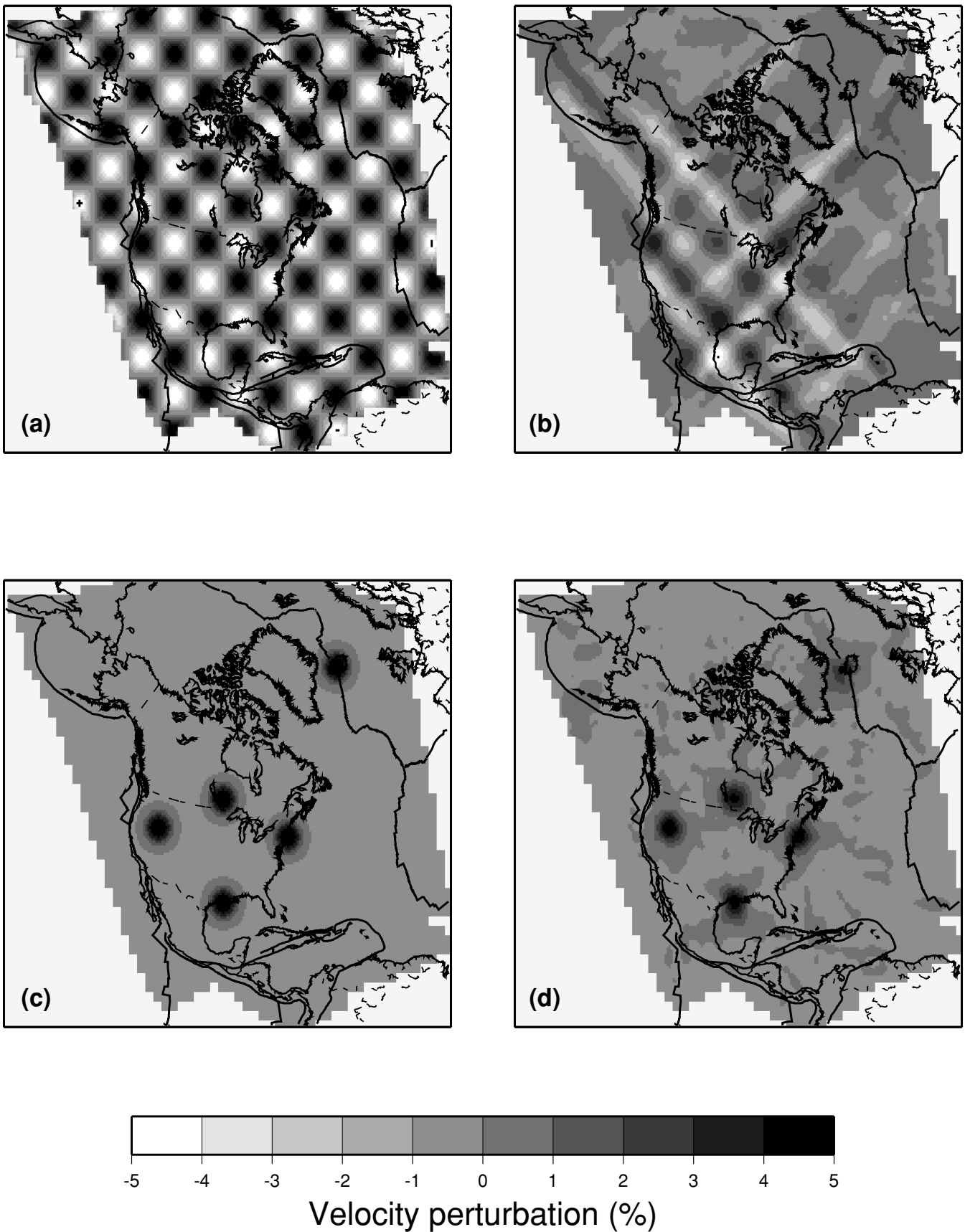


**Figure 4.** Results of the resolution tests: input (a, c) and output (b, d) velocity maps of the sensitivity tests for the period band 66–88 s. (a, b) checkerboard test with 8° cell size; (c, d) spike test.

**Table 1.** Variance reduction.

Period band (s)	Variance reduction (per cent) <sup>a</sup>	Variance reduction (per cent) <sup>b</sup>
115–150	75.2	42.7
88–115	64.9	32.4
66–88	61.6	14.3
50–66	41.8	–40*

<sup>a</sup>Obtained for our phase velocity maps.

<sup>b</sup>Obtained for phase velocity maps with amplitude reduced to 33 per cent.

\*Negative variance reduction indicates that the output synthetics present a poorer fit to the data than the input synthetics (PREM).

generally agree with previous regional surface wave studies (e.g. Alsina *et al.* 1996; Van der Lee & Nolet 1997; Frederiksen *et al.* 2001), but we provide new information across a larger area of North America, which includes the entire western Cordillera, the Canadian Shield, Alaska and the Caribbean basin.

The phase velocity maps display a remarkable consistency across North America for all periods (Fig. 6). Although the resolution tests show that we are able to image anomalies of at least 800 km, the average length-scale of the features observed in our models is larger than 1000 km. The two most prominent features imaged in our models are the relative high velocities (+3–5 per cent) present beneath northeastern North America and the slower velocities (–3 to –6 per cent) imaged beneath the active western margin of North and Central America. The two anomalies are well resolved and extend over all periods with a maximum contrast of 10 per cent at short periods to a lower value of 6 per cent at long periods. The high velocities beneath cratonic North America reflect an old and cooler upper mantle. These two velocity structures are consistent with global models (Trampert & Woodhouse 1995; Bijwaard & Spakman 2000; Larson & Ekström 2001) and regional studies (Grand 1994; Alsina *et al.* 1996; Van der Lee & Nolet 1997).

Depending on the period, the phase velocity perturbations observed can be related to Earth structure at different depths. For short periods (less than 50 s), Rayleigh waves are sensitive primarily to crustal structures, while at longer periods they sample the upper mantle from 50 to 300 km. This allows the interpretation of the phase velocity maps in terms of shear velocity structure. Beneath the Canadian shield and the northeastern United States, we observe fast velocity anomalies of up to +7 per cent. At long periods, the amplitude decreases to 2 per cent, suggesting that the craton extends down to 150 km. Besides the two main anomalies that characterize continental North America, small-scale features are also imaged. A weak lower-velocity feature (–1 per cent) is observed at long periods along the eastern Atlantic coast of North America from the Florida peninsula to 45°N (Figs 6a,b) and suggests low shear velocities at a depth of approximately 200 km. This feature in our model does not remain at shallower depths, as observed by Van der Lee & Nolet (1997), and does not extend to the Appalachians as inferred by Frederiksen *et al.* (2001).

The second dominant feature observed below the western Cordillera presents strong negative perturbations (–6 per cent) from the Aleutian Islands to Panama, which are associated with the active tectonic processes in the area. Beneath Alaska, this feature persists at long periods along the west coast owing to warm mantle materials. Along the Pacific coast of Canada, smaller amplitudes (–2 per cent) are observed at short periods. In the western United States, it is a broad structure of –5 per cent expanding into the interior, to the Basin and Range province. No specific low-velocity signa-

ture is observed beneath Yellowstone, unlike in the model of Van der Lee & Nolet (1997). Alsina *et al.* (1996) interpret relative high velocities of approximately +2–3 per cent (50–100 s period band) beneath the western United States (between 120°W and 125°W) as the subducted Juan de Fuca Plate in western Washington. However, in our model, clear low velocities are observed beneath this region. This discrepancy can be explained by the fact that the region lays at the edge of their model where lower resolution is expected.

In Mexico and Central America, we also observe slow heterogeneities in relation to the complex tectonic activity and volcanism in the region. At short periods, low velocities are observed down to Panama and Nicaragua, as a consequence of a warmer than average mantle. The Gulf of Mexico is imaged at short periods (50–60 s) as a low-velocity zone of –1 to –2 per cent, owing to the effect of a thick sedimentary basin. The recent work of Bassin *et al.* (2000) displays low phase velocities in the Gulf of Mexico, and the study of Vdovin *et al.* (1999) also shows low group velocities in the region, particularly for periods shorter than 50 s. The crust of the Caribbean basin is younger than the adjacent Atlantic Ocean, and it is surrounded by subduction zones, leading to relatively slower phase velocities. The Caribbean Plate is made of the Venezuelan and Colombian basins separated by the Beata ridge (Burke *et al.* 1978). The Venezuelan basin is characterized by faster anomalies (+1 per cent) relative to the Colombian basin, which is underlain by slower velocities anomalies (–2 per cent). This velocity differentiation agrees with the anomalously thick oceanic crust observed in the region related to the basaltic flow episode that took place in the pre-Mesozoic (80 Ma). In the eastern part (Venezuelan basin), thinner crust, similar to average oceanic crust is observed (Diebold *et al.* 1981) and the velocity signature is similar to the Atlantic Ocean. Thicker crust is reported in the Colombian basin leading to lower velocity anomalies. The persistence of this feature at long periods suggest that it extends through the upper mantle.

Relative slow velocities of –1 to –3 per cent are observed beneath Iceland and off the southeastern coast of Greenland. These relatively low velocities are attributed to a warm upper mantle and crust at the Mid-Atlantic ridge and the Iceland hotspot. Relative low-velocity anomalies beneath Iceland are weaker at longer periods. The resolution in this region is lower, as shown by the chequerboard and spike tests, and no information on the extent of the hotspot at larger depths can be inferred from our models. Along the eastern edge of the North American Plate, the Atlantic basin is characterized by relative high velocities (+2 to +3 per cent), while relative low velocities are present below the Mid-Atlantic Ridge. These slow velocities are clearly seen at shorter periods (66–88 s, corresponding to depths of 50–120 km), but diminish and become wider at longer periods.

## 6 DISCUSSION

### 6.1 Phase prediction: comparison of global and regional models

Our results show similarities with the recent global phase velocity model of Trampert & Woodhouse (2001), hereafter referred to as TW01. Using 46 000 Rayleigh wave measurements recorded primarily by GSN and Geoscope stations, they computed global phase velocity maps in the period range 40–150 s. Shown in Fig. 7 are the phase velocity maps of TW01 for periods of 60 and 130 s using a spherical harmonic expansion up to degree and order 40. The phase

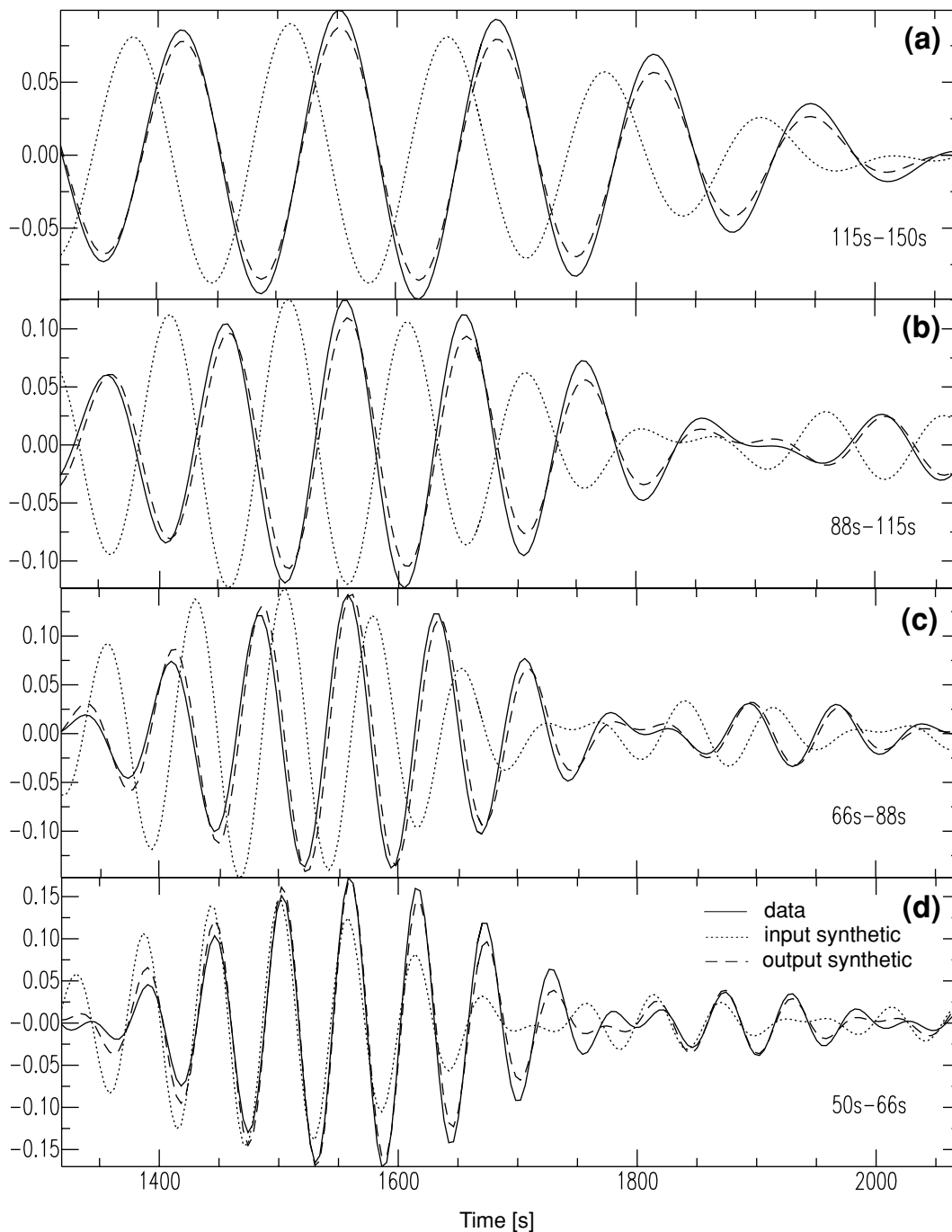


**Figure 5.** Waveform fits for the Colombia event of 1995 February 8 ( $M_w = 6.4$ ) recorded by station CMB (California). Solid lines, data; dotted lines, synthetic seismograms computed through the laterally homogeneous model PREM (input seismograms); dashed lines, output synthetic seismograms after waveform inversion.

velocity maps given in TW01 are obtained for narrow frequency bands (2.5 mHz wide) around a number of central frequencies. Therefore, we compare our maps for a period band (e.g. 115–150 s) with TW01 maps at the closest central period (e.g. 130 s). Major features, such as the large velocity contrast between the North American craton and the western Cordillera are clearly observed in both models. A comparison of the two models for periods of 50–100 s shows good agreement in both amplitude and lateral variations in phase velocities. The correlation between our model and TW01, computed over the whole inversion region, displays values

of 70 per cent at short periods (Table 2). For periods greater than 100 s, the agreement between the two maps (Fig. 7) is good, but the amplitude of the anomalies differs by approximately a factor of 3 and the correlation decreases to 46 per cent. For shorter periods, although the correlation between the two maps is good, a significant difference is observed in the Gulf of Mexico and the Caribbean basin. One of the new results obtained in our study is the slow-velocity region imaged beneath the Gulf of Mexico and the Caribbean Plate. While both models show slower velocities for the western part of the Caribbean basin, our results suggest large

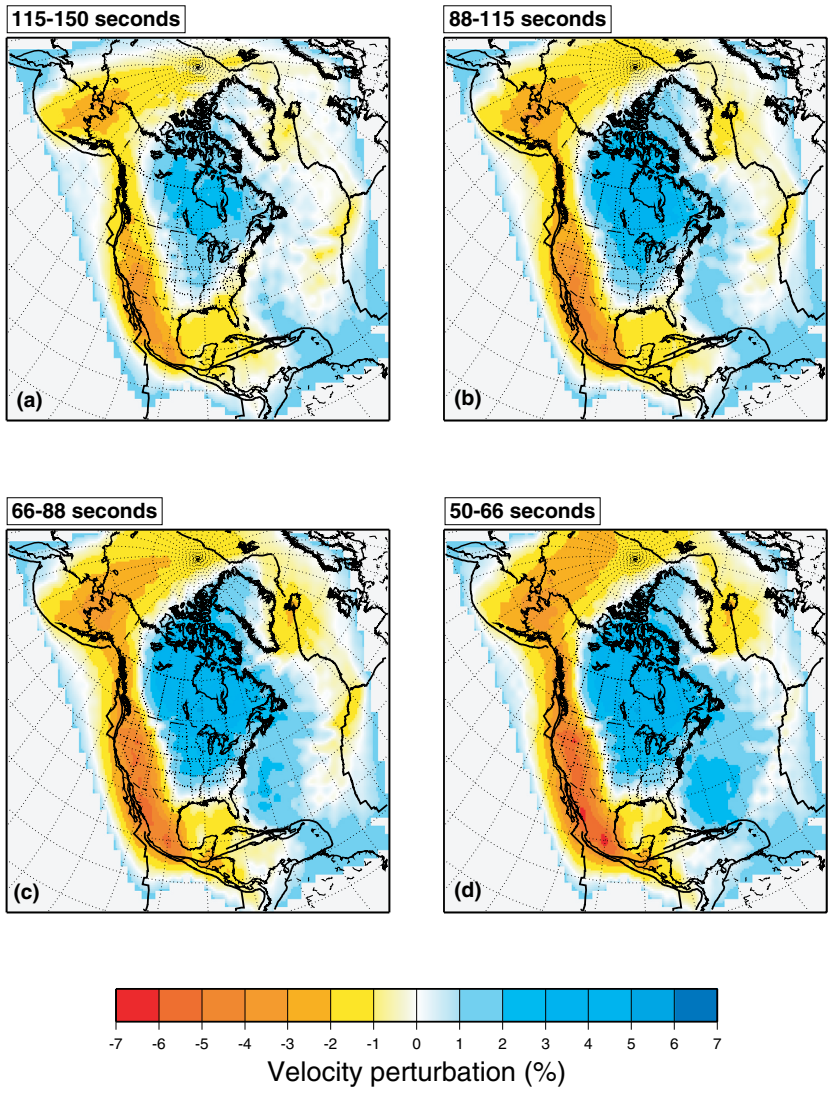


Figure 6. Estimated phase velocity maps after inversion for: (a) 115–150 s, (b) 88–115 s, (c) 66–88 s, (d) 50–66 s.

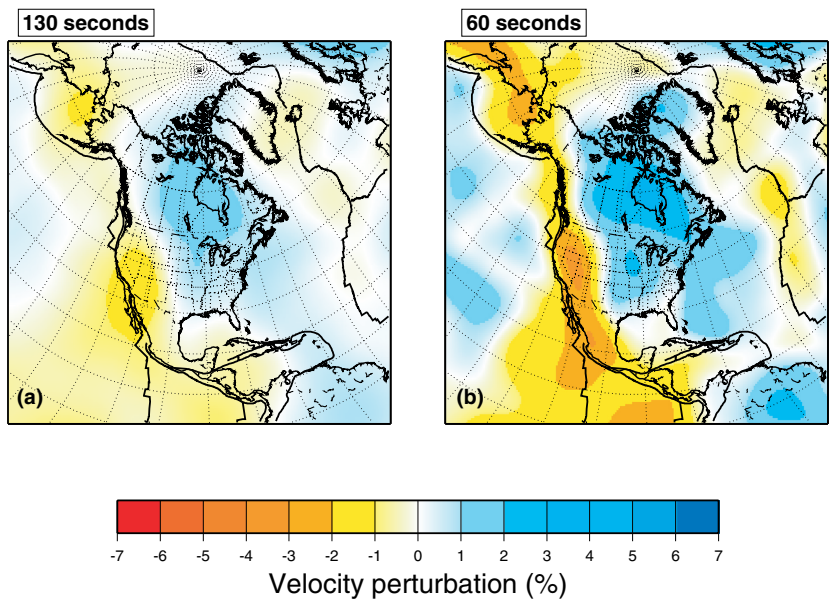


Figure 7. Phase velocity maps from Trampert & Woodhouse (2001) at (a) 130 s and (b) 60 s.

**Table 2.** Correlation between our regional model and the global model TW01.

Period band	Correlation (per cent)
115–150	46.1
88–115	66.0
66–88	71.1
50–66	70.9

variations between the western and eastern portions of the basin. Differences also occur along the edges of our model, where we lack ray coverage.

To determine the influence of the differences in the amplitude of the velocity anomalies on the data fit, we compute the variance reduction for a velocity model identical to that obtained by inversion, but with the amplitude of the anomalies reduced to one-third. A large decrease of the variance reduction is observed at all periods (right-hand column of Table 1). For the shortest periods (50–66 s), the synthetic seismograms exhibit poorer fit to the data than the PREM

seismograms, showing the importance of imaging accurately the amplitude of the velocity perturbations. The factor of 3 in amplitude observed between our model and TW01 is therefore significant and suggests that global models underestimate phase velocities at long periods. This may be attributed to the strong regularization applied in TW01 to compensate for noisy global data. Other surface wave global studies (Zhang & Lay 1996; Ekström *et al.* 1997) report lower amplitude at long periods than regional models. Larson & Ekström (2001) for Nolet *et al.* (1986) previously investigated the underestimation of velocity anomalies by global models in comparison with regional models. They suggest that the observed discrepancy may be caused by three reasons: the different phase velocity measurement techniques used in the global and regional inversions; the variable signal-to-noise ratio observed especially for short path-lengths; and the damping parameters applied.

The accurate estimation of phase arrival times is an important application of phase velocity maps. It is particularly relevant for moment tensor methods that use surface wave waveforms. In order to investigate the accuracy of our regional model and TW01 in predicting phase arrival times, we perform a forward modelling test. A

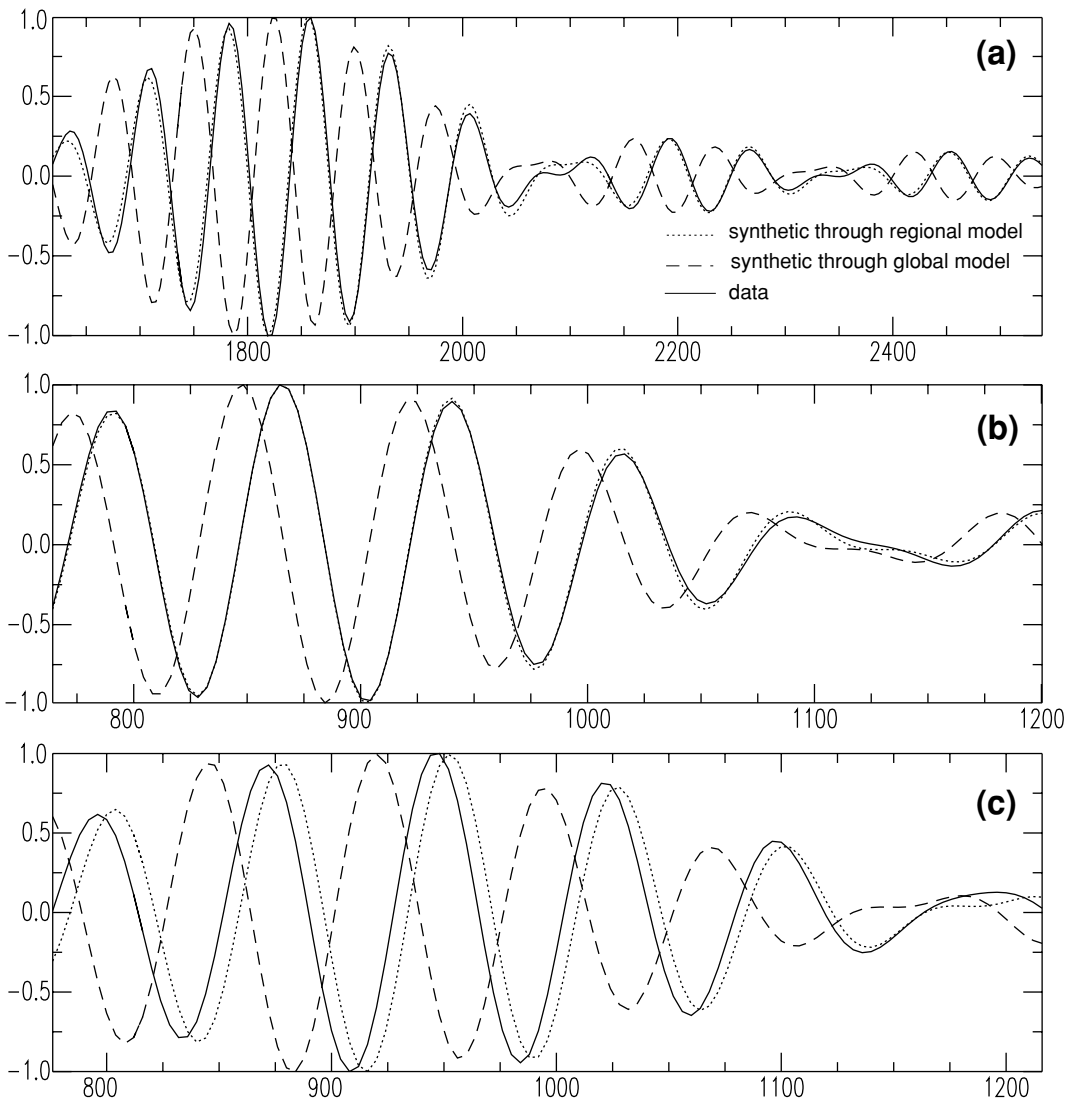


**Figure 8.** Comparison between normalized waveform predictions for our regional model (dotted line) and for the global model TW01 (dashed line). Northern Mid-Atlantic event of 2000 October 5 ( $M_w = 6.1$ ), recorded by station YBH (California) (a), Gulf of California event of 2000 March 24 ( $M_w = 5.4$ ), recorded by station SSPA (Pennsylvania) (b), Jalisco event of 2000 February 21 ( $M_w = 5.3$ ), recorded by station NEW (Washington State) (c).

total of 100 seismograms from eight events recorded in 2000 (stars in Fig. 1), which were not included in our inversion data set, were processed using the same method described in Section 2 (measurement of the group velocity followed by a phase-matched filter to isolate the fundamental mode). The waveforms are compared with the predicted seismograms computed by forward propagation through the two phase velocity maps (regional and global). As TW01 was obtained by inverting phase velocities measured from normalized seismograms, we compare the predictions in terms of normalized waveforms.

Examples of the predictions obtained are given on Fig. 8 for three different seismograms at 80 s period. The synthetics computed through the two models exhibit significant differences. Predictions computed through TW01 present phase arrival time differences of almost 25 s, while the time differences displayed by the regional predictions do not exceed 10 s. From the 100 seismograms used for this test, 97 were better predicted by our regional velocity map. Moreover, stronger discrepancies would be observed if true waveforms (not normalized) were compared. Almost 60 per cent of the synthetics computed through our regional model explain the data with rms residuals of between 0 and 0.4 (the root mean square of the difference between the observed and the predicted normalized waveforms). In contrast, the minimum rms residual observed for TW01 synthetics is 0.9. In Fig. 9, the rms residual averaged over all seismograms is displayed as a function of period. The discrepancy between the two sets of predictions is significant. The average rms residual obtained with our regional model is always lower than 0.6 for all periods, while for TW01 it reaches values of 3.2. This shows that despite the similarity observed between the two phase velocity maps, slight variations in velocity structures are important to explain the data. This is also supported by the systematic comparison of phase velocity models made by Trampert & Woodhouse (2001). Therefore, to obtain accurate phase predictions, it is essential to use regional phase velocity maps. This is particularly important for a regional moment tensor calculation (Arvidsson & Ekström 1998). The phase velocity maps of North America obtained in this study, which predict phase shifts with better accuracy, should significantly improve the CMT determination in the region.

### 6.2 Limitations of ray theory

The previous sections showed that we are able to reconstruct velocity features with better accuracy than global models (which has been illustrated for the TW01 model) and obtain better or comparable resolution than previous regional models (Alsina *et al.* 1996; Van der Lee & Nolet 1997; Frederiksen *et al.* 2001). However, the length-scale of the velocity features actually observed in the phase velocity maps is larger than expected from the synthetic tests (800 km). In order to understand the reasons why we do not obtain models with smaller features, we need to consider the approximations used in the inversion of the surface waves between 50 and 150 s. Our method is based on ray theory and assumes that the ray path follows the great circle linking the source and the receiver. In ray theory, the wave that travels through an inhomogeneous medium is assumed to be sensitive to velocity perturbations along the raypath. In reality, the wave is also sensitive to and becomes scattered by structures off the great circle. For example, Laske (1995) showed that using off-great-circle arrival angles from polarization analysis improves significantly the fit of long-period surface waves. If we take scattering effects into account in the forward direction (Snieder 1988), we can define scattering kernels (or Fréchet kernels) as the sensitivity of the wave to velocity perturbation at any geographical point (Marquering *et al.* 1998; Snieder & Lomax 1996; Dahlen *et al.* 2000; Hung *et al.* 2000). An example of a phase velocity sensitivity kernel is shown in Fig. 10, computed using the formalism described in Spetzler *et al.* (2002). The equivalent behaviour of the delay time is reported by Nolet & Dahlen (2000) using a Gaussian beam solution. Constructive interference at the receiver occurs for the waves scattered by anomalies inside a region defined as the first Fresnel zone that corresponds to the width of the main peak in Fig. 10 (e.g. Kravstov & Orlov 1990; Spetzler & Snieder 2001). It is an ellipsoidal area along the source–receiver path with a maximum width given by

$$L_F = \sqrt{\frac{3\lambda}{2} \tan \frac{\Delta}{2}}. \tag{3}$$

The maximum width of the Fresnel zone ( $L_F$ ) increases with the period ( $T = \lambda/v$ ) and the epicentral distance  $\Delta$ . For more details on the

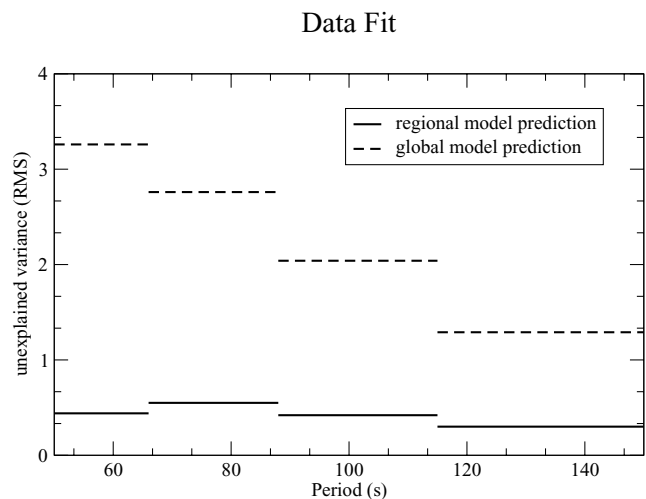


**Figure 9.** Comparison of the phase prediction for regional (solid line) and global (dashed line) models: root mean square of unexplained variance with the data after forward modelling. A total of 100 seismograms recorded in 2000 were used to compute the mean.

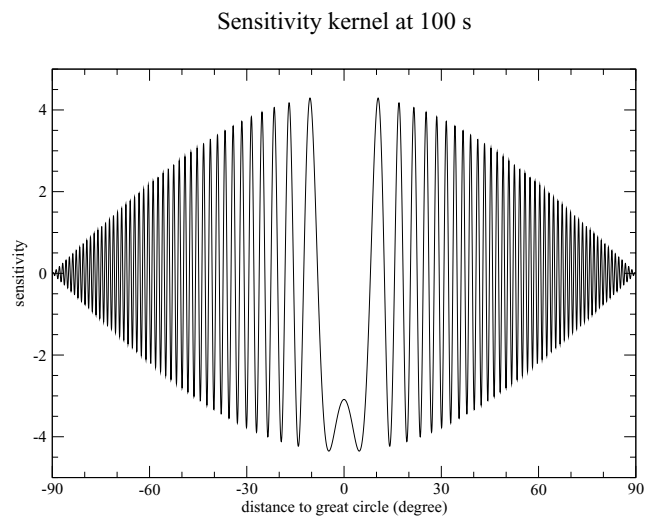


**Figure 10.** Cross-section of the scattering sensitivity kernel for relative phase velocity perturbations using finite frequencies. The epicentral distance is 100°, the view point is 50° away from the source along the great circle and the frequency is 100 s.

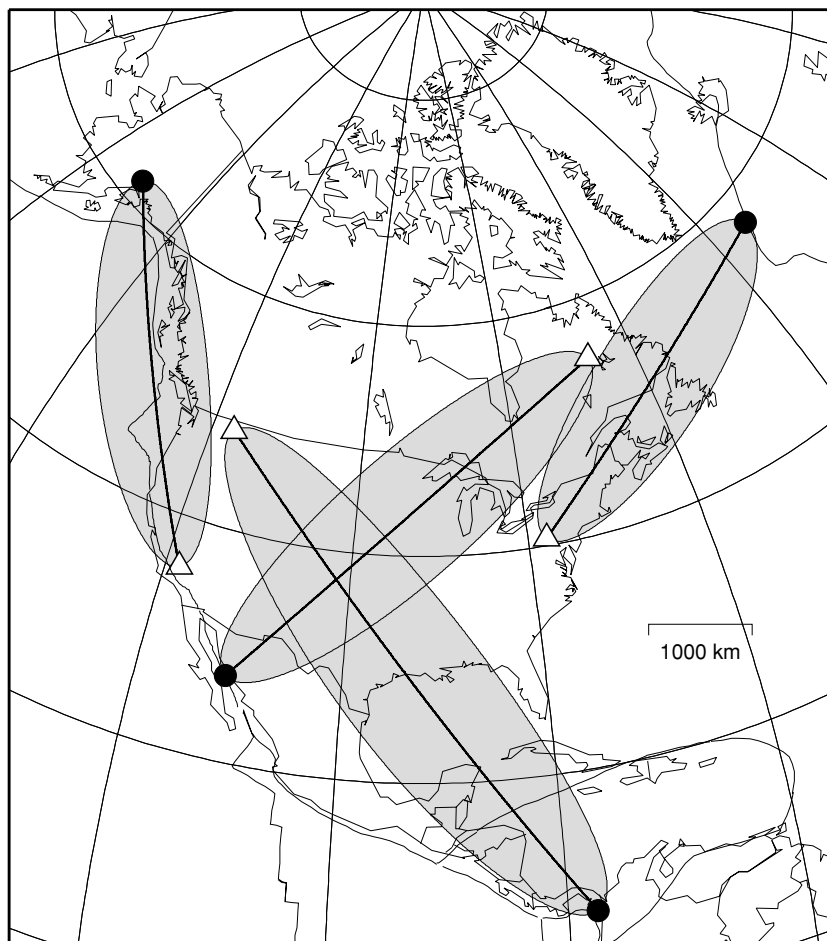


Figure 11. Fresnel zone width for four different paths at 100 s period. The width is computed using eq. (3).

derivation of sensitivity kernels and width of the Fresnel zone using the Rytov approximation in a uniform medium, we refer to Spetzler *et al.* (2002). In our study, at 100 s period, the Fresnel zone width can be as large as 1860 km for an epicentral distance of 10 000 km (Fig. 11). Inversions based on ray theory allow for reconstruction of velocity perturbations only along the raypath. For velocity perturbations much larger than the width of the Fresnel zone ( $a \gg L_F$ , where  $a$  is the characteristic length of the heterogeneity), the velocity reconstruction obtained using scattering theory is equivalent to that computed with ray theory but for structures of the order of or smaller than this width ( $a \lesssim L_F$ ), ray theory is no longer applicable.

To understand the consequences of diffraction effects on phase velocity structure imaging, Spetzler *et al.* (2001) computed the bias induced by diffraction on phase velocity measurements and compared it with the relative measurements error (see Fig. 2 in Spetzler *et al.* 2001). For a surface wave of 150 s, the error induced by the use of ray theory is not significant for velocity perturbations larger than 1250 km but is already of the order of 50 per cent for velocity perturbations of 1000 km. Recently, Yoshizawa & Kennett (2002) suggested that the zone of influence (e.g. the region to which a wave is sensitive to velocity anomalies) around the surface wave path is only one-third of the first Fresnel zone if the frequency range of the wave and the lateral heterogeneities of the medium are taken into account. The influence of scattering effects would then be limited to a smaller region around the geometrical ray, and the errors computed by Spetzler *et al.* (2002) would be overestimated. However, in our

continental-scale tomographic study, the features we are interested in have a length-scale for which scattering has a major effect. It is clear that expanding the data set without reformulating the inversion method used is not enough to obtain high-resolution models. The concern of future studies should be focused on accurate and realistic inversion procedures that take into account off-great-circle propagation and scattering effects.

## 7 CONCLUSIONS

Regional Rayleigh wave phase velocity maps were produced in the period range 50–150 s for North America and the Caribbean. These maps predict phase delays and long-period velocity amplitudes with higher accuracy than global models and are therefore reliable for source mechanism estimation or as starting model to *S*-wave structure studies. Despite significant improvements in data coverage and lateral resolution compared with previous investigations of the region, the ray theory approximation is a limiting factor for reconstructing short-wavelength structures. For the scale of velocity features we aim to image, off-great-circle propagation and scattering might be important. The influence of scattering effects in regional tomography requires further evaluation. The implementation of diffraction kernels in inversion procedures will determine whether a higher-order wave propagation approximation is necessary. These results have broad implications for proposed large-scale

seismic experiments in North America. A significant increase in station density may not translate into better models without improving the methodological assumptions and limitations.

## ACKNOWLEDGMENTS

We thank Bob Woodward and the USGS's Albuquerque SeismoLab for their help in data processing and knowledge of the inversion method. We are grateful to Charles Ammon for providing his code PGSWMFA for waveform filtering. We wish to thank the IRIS, Geoscope, USNSN, CNSN, Berkeley and SCEC teams for the data used in this study. Guust Nolet and an anonymous reviewer are also thank for their helpful comments. The investigations were (in part) supported by the Netherlands Geosciences Foundation (GOA) with financial aid from the Netherlands Organizations for Scientific Research (NWO) through the project 750.297.02.

## REFERENCES

- Alsina, D., Woodward, R.L. & Snieder, R., 1996. Shear wave velocity structure in North America from large-scale waveform inversions of surface waves, *J. geophys. Res.*, **101**, 15 969–15 986.
- Arvidsson, R. & Ekström, G., 1998. Global CMT analysis of moderate earthquakes,  $M_w$  4.5, using intermediate-period surface waves, *Bull. seism. Soc. Am.*, **88**, 1003–1013.
- Bassin, C., Laske, G. & Masters, G., 2000. The current limits of resolution for surface wave tomography in North America, *EOS, Trans. Am. geophys. Un.*, **81**, F897.
- Bijwaard, H. & Spakman, W., 2000. Nonlinear global P-wave tomography by iterated linearized inversion, *Geophys. J. Int.*, **141**, 71–82.
- Burke, K., Fox, P.J. & Sengör, A.M., 1978. Buoyant ocean floor and the evolution of the Caribbean, *J. geophys. Res.*, **83**, 3949–3954.
- Chevrot, S., Montagner, J.P. & Snieder, R., 1998. The spectrum of tomographic earth models, *Geophys. J. Int.*, **133**, 783–788.
- Curtis, A., Trampert, J., Snieder, R. & Dost, B., 1998. Eurasian fundamental mode surface wave phase velocities and their relationship with tectonic structures, *J. geophys. Res.*, **103**, 26 919–26 947.
- Dahlen, A., Hung, S.H. & Nolet, G., 2000. Fréchet kernels for finite-frequency traveltimes I. theory, *Geophys. J. Int.*, **141**, 157–174.
- Diebold, J.B., Stoffa, P.L., Buhl, P. & Truchan, M., 1981. Venezuela basin crustal structure, *J. geophys. Res.*, **86**, 7901–7923.
- Dziewonski, A.M. & Anderson, D.L., 1981. Preliminary reference Earth model, *Phys. Earth planet. Inter.*, **25**, 25 297–25 356.
- Dziewonski, A.M., Ekström, G. & Salganik, M.P., 1992. Centroid-moment tensor solutions for July–September 1991, *Phys. Earth planet. Inter.*, **72**, 1–11.
- Ekström, G., Tromp, J. & Larson, E.W.F., 1997. Measurements and global models of surface wave propagation, *J. geophys. Res.*, **102**, 8137–8157.
- Frederiksen, A.W., Bostock, M.G. & Cassidy, J.F., 2001. S-wave velocity structure of the Canadian upper mantle, *Phys. Earth planet. Inter.*, **124**, 175–191.
- Grand, S.P., 1994. Mantle shear structure beneath the Americas and surrounding oceans, *J. geophys. Res.*, **99**, 11 591–11 621.
- Hung, S.H., Dahlen, A. & Nolet, G., 2000. Fréchet kernels for finite-frequency traveltimes II. Examples, *Geophys. J. Int.*, **141**, 175–203.
- Kravtsov, Y.A. & Orlov, Y.I., 1990. *Geometrical Optics of Inhomogeneous Media*, Springer-Verlag, New York.
- Larson, E.W.F. & Ekström, G., 2001. Global models of surface wave group velocity, *Pure appl. Geophys.*, **158**, 1377–1399.
- Laske, G., 1995. Global observation of off-great-circle propagation of long-period surface waves, *Geophys. J. Int.*, **123**, 245–259.
- Levander, A., Humphreys, E.D., Ekström, G., Meltzer, A.S. & Shearer, P.M., 1999. Proposed project would give unprecedented look under North America, *EOS, Trans. Am. geophys. Un.*, **80**, 250–251.
- Lévêque, J.-J., Rivera, L. & Wittlinger, G.W., 1993. On the use of checkerboard test to assess the resolution of tomographic inversions, *Geophys. J. Int.*, **132**, 313–318.
- Levshin, A.L., Ratnikova, L. & Berger, J., 1992. Peculiarities of surface wave propagation across Central Asia, *Bull. seism. Soc. Am.*, **82**, 2464–2493.
- Levshin, A.L., Ritzwoller, M.H., Barmin, M.P., Villaseñor, A.V. & Padgett, C.A., 2001. New constraints on the Arctic crust and uppermost mantle: Surface wave group velocities,  $p_n$  and  $s_n$ , *Phys. Earth planet. Inter.*, **123**, 185–204.
- Marquering, H., Nolet, G. & Dahlen, F.A., 1998. Three-dimensional waveform sensitivity kernels, *Geophys. J. Int.*, **132**, 521–534.
- Nolet, G., 1990. Partitioned waveform inversion and two-dimensional structure under the network of autonomously recording seismographs, *J. geophys. Res.*, **95**, 8499–8512.
- Nolet, G. & Dahlen, F.A., 2000. Wave front healing and the evolution of seismic delay times, *J. geophys. Res.*, **105**, 19 043–19 054.
- Nolet, G., van Trier, J. & Huisman, R., 1986. A formalism for non-linear inversion of seismic surface waves, *Geophys. Res. Lett.*, **13**, 26–29.
- Nolet, G., Grand, S.P. & Kennett, B.L.N., 1994. Seismic heterogeneity in the upper mantle, *J. geophys. Res.*, **99**, 23 753–23 766.
- Pasyanos, M.E., Dreger, D.S. & Romanowicz, B., 1996. Toward real-time estimation of regional moment tensors, *Bull. seism. Soc. Am.*, **86**, 1255–1269.
- Pasyanos, M.E., Walter, W.R. & Hazler, S.E., 2001. A surface wave dispersion study of the middle East and North Africa for monitoring the Comprehensive Nuclear-Test-Ban Treaty, *Pure appl. Geophys.*, **158**, 1445–1474.
- Ritzwoller, M.H. & Levshin, A.L., 1998. Eurasian surface wave tomography: Group velocities, *J. geophys. Res.*, **103**, 4839–4878.
- Snieder, R., 1988. Large scale waveform inversion of surface waves for lateral heterogeneity, I, Theory and numerical examples, *J. geophys. Res.*, **93**, 12 055–12 065.
- Snieder, R. & Lomax, A., 1996. Wavefields smoothing and the effect of rough velocity perturbations on arrival times and amplitudes, *Geophys. J. Int.*, **125**, 796–812.
- Spetzler, J. & Snieder, R., 2001. The influence of small-scale heterogeneity on the travel time of waves, *Geophys. J. Int.*, **145**, 786–796.
- Spetzler, J., Trampert, J. & Snieder, R., 2001. Are we exceeding the limits of the great circle approximation in global surface wave tomography?, *Geophys. Res. Lett.*, **28**, 2341–2344.
- Spetzler, J., Trampert, J. & Snieder, R., 2002. The effect of scattering in surface wave tomography, *Geophys. J. Int.*, **149**, 755–767.
- Trampert, J. & Woodhouse, J.H., 1995. Global phase velocity maps of Love and Rayleigh waves between 40 and 150 seconds, *Geophys. J. Int.*, **122**, 675–690.
- Trampert, J. & Woodhouse, J.H., 2001. Assessment of global phase velocity models, *Geophys. J. Int.*, **144**, 165–174.
- USGS, 1999. *An Assessment of Seismic Monitoring in the United States: Requirement for and Advanced National Seismic System*, Vol. 1188, US Geological Survey Circular, p. 55.
- Van der Lee, S. & Nolet, G., 1997. Upper mantle S velocity structure of North America, *J. geophys. Res.*, **102**, 22 815–22 838.
- Vdovin, O., Rial, J.A., Levshin, A.L. & Ritzwoller, M.H., 1999. Group-velocity tomography of South America and the surrounding ocean, *Geophys. J. Int.*, **136**, 324–340.
- Woodhouse, J.H. & Dziewonski, A.M., 1984. Mapping the upper mantle: three dimensional modelling of Earth structure by inversion of seismic waveforms, *J. geophys. Res.*, **89**, 5953–5986.
- Yoshizawa, K. & Kennett, B.L.N., 2002. Determination of the influence zone for surface wave paths, *Geophys. J. Int.*, **149**, 440–453.
- Zhang, Y.-S. & Lay, T., 1996. Global surface wave phase velocity variations, *J. geophys. Res.*, **101**, 8415–8436.